Research Square

Preprints are preliminary reports that have not undergone peer review.
They should not be considered conclusive, used to inform clinical practice,
or referenced by the media as validated information.

Stromal Vegf-c Expression Predicts Nodal Metastasis and Supports De-escalation of Axillary Surgery in Breast Cancer

Pauline Jeannot
Lund University
Emelie Edvardsson
Lund University
Oscar Hernquist
Lund University
Cornelia Brandt
Lund University
Linnea Fischhaber
Lund University
Anna-Maria Larsson
Lund University
Beatrice Öhlund
Lund University
Pär-Ola Bendahl
Lund University
Charlotte Rolny
charlotte.rolny@med.lu.se
Lund University
Lisa Ryden
Skåne University Hospital

Article

Keywords:

Posted Date: March 31st, 2026

DOI: https://doi.org/10.21203/rs.3.rs-9086419/v1

License: This work is licensed under a Creative Commons Attribution 4.0 International License.
Read Full License

Additional Declarations: No competing interests reported.

Abstract

Accurate preoperative prediction of lymph node metastasis (LNM) is critical for de-escalating breast cancer surgery, sparing node-negative patients the morbidity of sentinel lymph node biopsy while ensuring appropriate staging for those at risk. Yet reliable molecular predictors of LNM remain lacking. VEGF-C, a key driver of lymphangiogenesis, is expressed in both cancer cell and stromal compartments, but its clinical utility is unclear. In a prospectively enrolled cohort, we assessed stromal and cancer cell VEGF-C expression by immunohistochemistry using both manual scoring and a novel automated image analysis script enabling objective, reproducible quantification of stromal versus epithelial VEGF-C fractions at scale. Stromal VEGF-C was independently associated with LNM after adjustment for established predictors (P = 0.004), with prediction models reaching AUCs of up to 0.784. Cancer cell VEGF-C added no predictive value. Critically, stromal VEGF-C showed potential to replace vascular invasion, which is a strong but preoperatively inaccessible predictor in LNM prediction models. Stromal VEGF-C assessment in preoperative biopsies could therefore enable more precise nodal staging, supporting informed surgical decision-making and the identification of patients who may safely avoid unnecessary axillary intervention.

INTRODUCTION

Sentinel lymph node biopsy (SLNB) offers a less invasive method of axillary staging in breast cancer compared with axillary lymph node dissection (ALND), resulting in fewer complications [1]. However, SLNB is not entirely free of morbidity, as some patients still experience lymphedema, pain, or reduced arm mobility. As the proportion of patients with nodal metastases detected by SLNB has declined, recent trials such as SOUND[2] and INSEMA[3] have demonstrated that omission of SLNB in selected low-risk patients does not compromise oncologic outcomes, suggesting axillary surgery may be safely omitted in carefully chosen cases [2,3]. Nonetheless, reliable non-invasive methods are needed to identify patients unlikely to harbor lymph node metastases (LNM). To address this, we developed NILS (Non-Invasive Lymph Node Staging), a decision support tool that uses an artificial neural network trained on clinical and pathological data to estimate the probability of node-negative disease [4]. The model incorporates ten key clinicopathological variables, including patient factors (age and mode of detection) and tumor characteristics (tumor size, location, multifocality, histopathological type, estrogen receptor [ER] and progesterone receptor [PR] status, cancer cell proliferation (Ki-67), and vascular invasion [VI]). Upon external validation, NILS has achieved an AUC of 0.67 (95% CI: 0.62-0.72), allowing approximately 26% of patients to safely avoid axillary surgery while maintaining 90% sensitivity [5].

Because some of the variables in the NILS model, particularly VI, are inconsistently reported and/or challenging to assess preoperatively, additional biomarkers are being investigated to improve the model's predictive accuracy. Recent evidence indicates that VEGF-C–expressing tumor-associated macrophages (TAMs) promote lymphatic rather than hematogenous spread, thereby increasing lymph

node involvement[6]. Stromal VEGF-C expression, particularly in TAMs, may therefore be a promising biomarker for predicting LNM and enhancing non-invasive axillary staging prediction models.

RESULTS

Stromal-, but Not Cancer Cell–Derived, VEGF-C is associated with Lymph Node Metastasis by Semi-Quantitative Scoring

To evaluate whether stromal and/or cancer cell derived VEGF-C expression could serve as a predictive biomarker for LNM, VEGF-C expression in both compartments was evaluated by immunohistochemistry. Fig. 1A shows a flow chart illustrating the selection of patients for this project from the original 564 women enrolled in the BMM cohort. VEGF-C expression in stromal and cancer cells was manually quantified in primary tumor TMA cores from 440 patients in the BMM cohort (Fig. 1B, C), of which 411 fulfilled the predefined criteria for prediction of LNM**.** The patients excluded in this step would not have been eligible for upfront sentinel lymph node biopsy (SLNB). Table 1 summarizes the characteristics of this subset, overall and stratified by stromal fraction of VEGF-C. Briefly, the median age at breast cancer diagnosis was 57 years; 163 patients (40%) had node-positive disease (N+), 137 (33%) had T2 tumors, and 112 of 408 (27%) of the tumors were Nottingham histological grade (NHG) 3. VEGF-C stromal fraction was strongly associated with LNM, VI, tumor infiltrating lymphocytes (TILs), NHG, Ki-67, and age at diagnosis (Table 1). Also, VEGF-C expression in cancer cells was associated with multiple clinicopathological variables (age, VI, ER- and PR-status, Ki67, histology grade and St Gallen classification), but it was not associated with nodal status (Table 2). High-intensity VEGF-C expression was observed in stromal, but not cancer cells. VEGF-C–high stromal cells were quantified as the proportion of VEGF-C–positive stromal cells, whereas cancer cell VEGF-C showed variable intensity and was scored using four intensity classes (Fig. 1B, C).

Novel Automated QuPath-Based Pipeline for Stromal and Cancer Cell Classification

A composite machine-learning classifier was applied to identify stromal and cancer cells (Fig. 1D, E) using the same parameters as the semiquantitative scoring (Fig. 1B, C). Concordance between manual and automated assessments was observed for stromal cell fractions (Spearman’s ρ = 0.67; Fig. 1F) and for cancer cell expression (Spearman’s ρ = 0.57; Fig. 1G). Importantly, the measurements from a dual pan-CK/VEGF-C immunofluorescence staining further validated precise compartmental separation (Fig. 1E, H, I). The usability of the automated script-based analysis for quantification of VEGF-C expression in stromal and cancer cells was further validated on TMAs with primary tumor samples from the CTC-MBC study. A flowchart outlining the number of patients with at least one assessable core in this cohort is presented in **Fig. 2A**. Consistent with the findings in the BMM cohort, automated quantification of VEGF-C expression in both stromal cells (Fig. 2B) and cancer cells (Fig. 2C) in the CTC-MBC cohort showed a strong correlation with manual scoring (Spearman’s ρ = 0.71 and 0.60, respectively; Fig. 2D, E). For script-based assessment in the BMM cohort, stromal VEGF-C fraction was associated with LNM (Table 1), whereas cancer cell VEGF-C intensity showed only a weak association (Table 2).

Stromal- derived VEGF-C as a novel predictor for lymph node metastasis

Associations to LNM were further quantified as odds ratios (OR) estimated using univariable logistic regression analysis (Table 3). For manual assessment of stromal VEGF-C fraction, the category without VEGF-C expression (fraction 0%) was chosen as reference. The odds of LNM increased by a factor of 2.09 [95% CI: 1.02-4.29 P = 0.045, (Table 3)] for the fraction 1-5%. The corresponding multiplicative factors for the two higher classes 6-25% and ≥26% were 3.45 (95% CI: 1.57-7.60) and 3.67 (95% CI: 1.41-9.56), respectively. Also, script-based analysis of stromal VEGF-C fraction was a strong predictor of LNM [OR 1.140; 95% CI: 1.011-1.286; P = 0.019 (Table 3)] per percentage point. The observed relationship between the log odds of LNM and stromal VEGF-C fraction was found to be non-linear. To address this, the fractions were post-hoc transformed using $\log_2$. The OR per doubling of the script-based VEGF-C-fraction was 1.212 (95% CI: 1.115-1.318; P < 0.001; Table 3). As anticipated, also tumor size, mode of detection, multifocality, and VI were strong predictors of LNM (Table 3). The evidence for association between cancer cell VEGF-C intensity and LNM was, however, very weak (P > 0.60) for both manual and script-based assessment.

As shown in Table 1, stromal VEGF-C is associated with multiple established predictors of LNM, suggesting that the crude ORs reported in Table 3 may be confounded. For example, patients lacking VEGF-C–positive stromal cells (fraction 0%, *n* = 49) had a median age of 66 years, which progressively decreased with increasing stromal VEGF-C fractions (P_{trend} < 0.001). To better approximate the causal association between stromal VEGF-C fraction and LNM, two multivariable logistic regression models were fitted—one per assessment method—adjusting for identified potential confounders (Table 4). The adjusted ORs for VEGF-C were of similar magnitude to the crude ORs in Table 3, indicating that the association with LNM remained robust after adjustment for established predictors. The association was particularly strong for the script-based assessment (P = 0.004), supporting its potential to improve nodal prediction models.

Integration of VEGF-C Into the NILS Predictive Model for Lymph Node Metastasis

We previously developed NILS, a multivariable artificial neural network (ANN)–based model for predicting LNM (4). The original model incorporated ten variables, ranked by decreasing influence: tumor size (mm), vascular invasion (VI; yes/no), multifocality (yes/no), ER status (+/−), histological type (NST/ILC/other), PR status (+/−), mode of detection (symptomatic/screening), age (years), tumor localization (four quadrants + central), and Ki67 (%).

To assess the potential added predictive value of stromal VEGF-C fraction, we derived a reference model — the NILS proxy — using logistic regression in the subset of the BMM cohort with complete data for both manual and script-based VEGF-C assessment (n = 377). Seven of the ten original NILS variables were retained; PR and location status were excluded due to substantial missing data, and Ki67 was replaced by NHG (grades I–III), which similarly reflects tumor proliferation but is more reliably assessed. The final complete-case model was built on n = 332 patients, with the reduction from 377 attributable

primarily to missing VI data. The NILS proxy achieved an AUC of 0.766. Incorporating semi-quantitative VEGF-C scoring improved this to 0.778, while script-based quantification yielded a further gain, reaching an AUC of 0.784 (Fig. 3A).

To evaluate the clinical utility of VEGF-C for predicting LNM, decision curve analysis (DCA) was performed. The Net Benefit of three models was calculated across a range of threshold probabilities: the NILS-proxy model, and the NILS-proxy model augmented with stromal VEGF-C fraction, using semi-quantative and script-based assessments, respectively (Fig. 3B). All the three models have higher Net Benefit than the two extreme alternatives, SLNB for all and SLNB for none, across a wide range of clinically relevant thresholds.

Since VI cannot be reliably assessed on core needle biopsies (12), we next examined whether VEGF-C scoring could serve as a substitute in nodal predictive models. Replacing VI with script-based VEGF-C fraction yielded a larger AUC gain (ΔAUC = 0.022), bringing the AUC to 0.772. Model comparison via Akaike's information criterion (AIC) further supported the added value of VEGF-C: its inclusion produced a greater improvement than VI alone (ΔAIC = 10.4 vs. 6.4), with the 4.0-unit difference surpassing the widely accepted threshold of 2 units for a meaningful distinction (13). Script-based stromal VEGF-C fraction was the second most influential predictor of LNM after tumor size and enabled inclusion of patients with missing VI, increasing the sample size from 332 to 366. In this expanded cohort, the NILS proxy model without VI but with script-based stromal VEGF-C achieved an AUC of 0.779. Results for manual VEGF-C fraction were similar.

Stromal-Derived VEGF-C Expression and Patient´s Prognosis

Since stromal VEGF-C fraction was shown to predict LNM, which is an established predictor of poor survival, we also investigated its association with overall survival. Kaplan-Meier estimates for each of the four categories of manually assessed stromal VEGF-C fraction and for quartiles of the script-based fraction are shown in Fig. 3C, D. A log-rank test for trend showed strongest evidence for association to overall survival for the manual assessment (P = 0.0085 versus P = 0.119). More specifically, the survival seems to be poor in the group lacking stromal VEGF-C expression (manual fraction 0%). A post hoc univariable Cox-regression contrasting this category with the other three categories combined, was used to quantify this crude multiplicative effect on survival. The hazard ratio (HR) was 1.91 (95% CI: 1.36-2.69), however, this estimate turned out to be confounded by age. Patients lacking stromal VEGF-C were, on average, 7.0 years older than those with a fraction ≥1%, resulting in an age-adjusted HR of 1.20 (95% CI: 0.84-1.71). The association between cancer cell VEGF-C intensity and overall survival was even weaker (data not shown). Associations to the endpoints breast cancer specific survival, recurrence-free survival and distant recurrence-free interval were in the same direction and of essentially the same magnitude (data not shown).

DISCUSSION

In this prospective–retrospective study of primary breast cancer patients, we demonstrate for the first time that stromal VEGF-C expression is an independent predictor of LNM, underscoring its potential as a novel biomarker for nodal staging. In contrast, VEGF-C expression in cancer cells showed no predictive value for nodal status. Importantly, script-based VEGF-C assessments yielded results comparable to manual scoring, supporting the feasibility of digital pathology for future clinical implementation. These findings are particularly relevant in the context of current efforts to de-escalate axillary surgery, and they highlight the critical importance of identifying the cellular source of a biomarker when evaluating its prognostic and clinical utility.

Over the past two decades, axillary management in breast cancer has shifted substantially, with ALND largely abandoned in favor of SLNB [7], which currently is also under scrutiny. Updated ASCO guidelines [8] recommend omission of SLNB in selected patients—postmenopausal women with clinical node-negativity, low-risk tumors undergoing breast-conserving surgery including radiotherapy and endocrine therapy—based on the SOUND (2) and INSEMA trials [3] which showed non-inferiority of omission. However, these trials excluded younger patients and those undergoing mastectomy, limiting generalizability of the findings. Consistent with ASCO guidelines, axillary omission should be individualized using risk models integrating tumor biology, patient preferences, and clinical stage. Current nodal prediction models rely mainly on clinical stage, as tumor phenotype, including ER status, adds limited value. Although VI strongly predicts nodal involvement, its limited assessment on core biopsies restricts preoperative use. Stromal VEGF-C may serve as a feasible surrogate for VI, improving preoperative nodal risk stratification and supporting safe de-escalation of axillary surgery. Stromal VEGF-C expression improved discrimination of the multivariable NILS model for LNM beyond established predictors. Although the AUC gain was modest, AUC is a stringent metric, particularly when the baseline model already shows good discrimination[8]. The gain of adding VEGF-C to the model was more evident when improvement was measured by AIC or a likelihood ratio test.

The observed dose–response relationship between increasing stromal VEGF-C fraction and the odds of LNM supports a potential causal association and is consistent with our prior work (5) demonstrating that VEGF-C–expressing TAMs promote lymphatic dissemination while concurrently normalizing tumor vasculature and limiting hematogenous spread. We show that absence of stromal VEGF-C was associated with worse survival in univariable analyses; however, this association was substantially attenuated after adjustment for age. Patients with stromal VEGF-C–negative tumors were, on average, seven years older than those with detectable stromal expression. These findings suggest that loss of stromal VEGF-C reflects age-associated remodeling of the tumor microenvironment rather than an independent prognostic determinant. Aging is known to alter stromal cell populations, including fibroblasts, endothelial cells, and TAMs, which undergo age-dependent phenotypic and functional changes [9]. Given the capacity of TAMs to produce and respond to VEGF-C, reduced stromal VEGF-C expression in older patients likely represents a feature of microenvironmental aging rather than a tumor-intrinsic driver of clinical outcome.

Key limitations include the retrospective assessment of VEGF-C in archival tumor material and the presence of non-assessable cores, which reduced the number of evaluable cases, particularly in complete-case analyses. Future studies should include larger cohorts, apply multiplex immunofluorescence to clarify the cellular origin of VEGF-C–positive stromal cells, and incorporate diagnostic core needle biopsies to support preoperative risk assessment.

In conclusion, stromal, but not cancer cell–derived, VEGF-C is an independent, dose-dependent predictor of lymph node metastasis in primary breast cancer. Using a novel automated script based digital pathology tool on a single immunohistochemical marker, stromal VEGF-C was quantified objectively and reproducibly in a large prospectively enrolled cohort with long-term follow-up, showing strong concordance with manual scoring in an independent validation cohort. This approach reduces observer bias, supports integration into modern pathology workflows, and highlights stromal VEGF-C as a promising biomarker to refine nodal staging and enable safe de-escalation of axillary surgery.

MATERIAL AND METHODS

Study cohorts

A total of 555 patients were included in the prospective bone-marrow metastasis (BMM) cohort, established to assess the prognostic significance of cytokeratin-positive cells in bone marrow [10]. Formalin-fixed, paraffin-embedded primary tumors were retrieved to construct tissue microarrays (TMAs) (7). Biomarker analyses included ER, PR, Ki-67, and HER2 status [11] and vascular invasion was retrospectively scored on whole-slide sections [12]. An independent validation cohort of 156 patients from a prospective study [13] of circulating tumor cells in metastatic breast cancer (CTC-MBC) was included for comparison of assessment protocols only [14]. Survival data were retrieved from Statistics Sweden ((https://www.scb.se/en/) in November 2024, and recurrence data were obtained from patient records. Only patients eligible for upfront SLNB (T1–T2, no neoadjuvant therapy) were included in LNM prediction analyses, while all patients with available VEGF-C scores were included in method concordance and prognostic analyses.

Ethics

All patients provided written informed consent at time of inclusion, and the studies were approved by the Ethics Committee at Lund University (LU699-09, LU75-02, and LU2010/35). Retrieval of outcome data from Statistics Sweden and individual patient files was approved in 2023 by the Swedish Ethics Review Authority (2023-01457-02 and 2023-03844-01).

Immunohistochemistry

Paraffin-embedded TMA blocks were sectioned into 4.0 µm slices using a Microm HM355S microtome (Thermo Fisher Scientific, Kalamazoo, MI, USA). Automated immunohistochemical (IHC) staining was performed using the Ventana Discovery Ultra platform (Roche Diagnostics Corp., Indianapolis, IN, USA),

including deparaffinization, antigen retrieval, and blocking of non-specific interactions. A monoclonal mouse anti-VEGF-C antibody (clone E6, sc-374628; Santa Cruz Biotechnology, Dallas, TX, USA) was used as the primary antibody, using a dilution of 1:100, incubated for 32 min at 37 °C. The secondary antibody was Discovery OmniMap HRP-conjugated anti-mouse (Roche Diagnostics, Solna, Sweden), incubated for 16 min at 37 °C. Signal detection was carried out using the ChromoMap DAB kit (Roche Diagnostics, Solna, Sweden). The protocol was optimized using tonsillar and breast tumor tissue, with lymphatic endothelial cells, mesothelial cells, reticular cells, and follicular dendritic cells serving as positive controls for VEGF-C staining. Slides containing TMA cores were scanned using a NanoZoomer S60 Digital Slide Scanner (Hamamatsu Photonics, Hamamatsu, Japan) and digitally analyzed with PathXL Xplore (Philips, Amsterdam, Netherlands) at 20× magnification. On average, two cores were assessed per patient, and the maximum score of matching cores was used in all analyses.

Manual scoring of VEGF-C expression

VEGF-C expression was independently assessed by two blinded evaluators using a predefined scoring protocol. A third assessor was involved in discordant cases. Exclusion criteria were missing or damaged cores, <50 invasive cancer cells, and cores containing only in situ lesions. Cytoplasmic VEGF-C staining in cancer cells was evaluated for both intensity (0 = negative; 1 = weak; 2 = moderate; 3 = strong) and fraction of positive cancer cells (0 = 0%; 1 = 1–5%; 2 = 6–25%; 3 = 26–50%; 4 = 51–75%; 5 ≥76%). The cancer cells were homogenously stained, why only intensity was considered for further analysis. Stromal cells, defined as non-epithelial, non-cancerous cells within the tumor microenvironment, were assessed according to the same criteria. However, since all stained stromal cells had a strong intensity, only the fraction of VEGF-C expressing stromal cells is reported in this study, and since only a single tumor had a VEGF-C fraction above 50%, the classes 3-5 were merged in all analyses. Blood vessels and muscle fibers were excluded from stromal scoring.

Script-based scoring (QuPath)

Digital images were imported into *QuPath* (version 0.5.1) [15]. Color deconvolution was optimized for each cohort to improve separation of the hematoxylin and DAB signals. For the BMM cohort, stain vectors were set to hematoxylin (0.73111, 0.59519, 0.33351) and DAB (0.34211, 0.5857, 0.73479) with a background value of (236, 231, 227). For the CTC cohort, stain vectors were set to hematoxylin (0.71817, 0.58684, 0.37398) and DAB (0.2286, 0.53372, 0.81418) with a background value of (235, 230, 226). TMA cores were automatically identified using QuPath's TMA dearrayer plugin (*qupath.imagej.detect.dearray.TMADearrayerPluginIJ*), with a target core diameter of 1.0 mm, a density threshold of 5, and a boundary scale of 105%. For the BMM cohort, multiple TMA slides with differing label orientations were processed using cohort-specific dearraying scripts. For the CTC cohort, a single dearraying configuration was applied. For both cohorts, manual adjustments were applied where automatic dearraying was suboptimal. Cores with >50% missing or damaged tissue, consisting solely of stromal tissue or out of focus were excluded from analysis. Tissue areas within each TMA core were segmented using the *Simple Tissue Detection* module

(*qupath.imagej.detect.tissue.SimpleTissueDetection2*). Detection was performed at a pixel size of 5.0 µm with an intensity threshold of 225 on a brightfield background. Regions smaller than 10,000 µm² were excluded, holes smaller than 1,000 µm² were filled, and image smoothing and median cleanup were applied prior to detection.

Nuclei detection was performed using the *Watershed Cell Detection* algorithm (*qupath.imagej.detect.cells.WatershedCellDetection*) based on the hematoxylin Optical Density (OD) channel. For the two cohorts, detection was performed at a requested pixel size of 0.5 µm, with a Gaussian sigma of 1.1 µm, a background radius of 12.0 µm (estimated by reconstruction). A hematoxylin OD threshold of 0.09 was applied to the BMM cohort and 0.15 to the CTC cohort. Detected nuclei were required to have an area between 8.0 and 150.0 µm². Cells were defined by expanding each detected nucleus by 1 µm, and all morphological measurements were recorded for downstream classification.

*Cell compartment classification — BMM cohort***.** To classify detected cells as stromal or cancer cells, a composite object classifier (*Combined_Size_Ecc_Hemato*) was applied in three sequential steps. First, an artificial neural network multilayer perceptron (ANN_MLP) classifier was trained using two nuclear features — nucleus area and nucleus hematoxylin OD mean — with a symmetric sigmoid activation function and Resilient Backpropagation (RPROP) training (up to 1,000 iterations, convergence threshold ε = 0.01). This classifier assigned cells to either a high-hematoxylin class (stromal) or tumor cell class. Second, a threshold-based classifier on nucleus eccentricity (threshold: 0.899) excluded elongated cells from the tumor cell class, reclassifying those with eccentricity ≥ 0.899 as non-tumor. Third, a threshold-based classifier on nucleus area (threshold: 14.0 µm²) excluded small nuclei from the tumor cell class, reclassifying those with area < 14.0 µm² as non-tumor. These three classifiers were applied sequentially as a composite pipeline to all detected cells.

VEGF-C expression quantification — BMM cohort. For each TMA core, VEGF-C staining intensity in cancer cells was quantified from the DAB OD channel and the mean DAB OD per cancer cell was calculated. In parallel, a second ANN_MLP classifier (*VEGFC_high*) was trained on cell-level DAB OD mean to classify stromal cells as VEGF-C high or VEGF-C low, using a symmetric sigmoid activation function and RPROP training (up to 1,000 iterations, ε = 0.01). The classifier was trained using annotation criteria aligned with manual scoring to ensure comparability between automated and manual assessments. The count of VEGF-C-high stromal cells was normalized to the total number of stromal cells per core to determine the fraction of VEGF-C expressing stromal cells.

Cell compartment classification — CTC cohort. For the CTC cohort, cell detection thresholds and classifier features were adapted to account for differences in tissue processing and staining. A composite classifier (*Size_Ecc_HematoX_filter*) was applied using the same three-step sequential architecture as the BMM cohort, but with an expanded feature set for the ANN_MLP step. Eight nuclear features were used: nucleus area, eccentricity, hematoxylin OD mean, sum, standard deviation, maximum, minimum, and range. The ANN_MLP used a symmetric sigmoid activation function with RPROP training (up to 1,000 iterations, ε = 0.01). Threshold-based filters were subsequently applied for

nucleus eccentricity (threshold: 0.923) and nucleus area (threshold: 14.0 μm²), using the same logic as the BMM cohort.

*VEGF-C expression quantification — CTC cohort***.** VEGF-C expression in stromal cells of the CTC cohort was quantified using a dedicated ANN_MLP classifier (*VEGFC_high*) trained on six nuclear DAB OD features: mean, sum, standard deviation, maximum, minimum, and range. This extended feature set, compared to the single DAB OD mean used in the BMM cohort, was employed to improve classification specificity given the different staining characteristics of the CTC tissue. The classifier used a symmetric sigmoid activation function with RPROP training (up to 1,000 iterations, ε = 0.01) and output cells as VEGF-C high or VEGF-C low. The classifier was trained using annotation criteria aligned with manual scoring to ensure comparability between automated and manual assessments. The fraction of VEGF-C expressing stromal cells was calculated as in the BMM cohort.

*Validation of compartment-specific scoring***.** To validate compartment-specific classification, TMAs were co-stained with a pan-cytokeratin antibody (CKAE1/3, #M3515, Agilent Technologies, Santa Clara, CA, USA; M3515) together with the VEGF-C antibody sc-374628 (Santa Cruz biotech) employing the NEL871001KT Opal 6-Plex Detection Kit Opal 520 for Vegfc and TSA-DIG for CKPAN (Akoya Bioscience) and imaged using a PhenoImager HT instrument (Akoya Bioscience). This multiplexed approach allowed direct assessment of the correspondence between QuPath-classified cancer cells and cytokeratin-positive cells.

All QuPath scripts and trained classifiers for both the BMM and CTC cohorts, including color deconvolution settings, TMA dearraying configurations, tissue and cell detection parameters, composite cell classification pipelines, and VEGF-C scoring classifiers, have been deposited at https://github.com/rolnylab/Jeannot-Edvardsson-BreastCancer-Stromal-VEGFC-LymphNode/tree/main; DOI link found at https://doi.org/10.5281/zenodo.18803748

Statistical methods

Associations between the manually assessed fraction of VEGF-C-expressing stromal cells and clinicopathological variables were summarized using median and range for continuous variables and percentages for categorical or of no association to VEGF-C was evaluated using a test of zero slope in a linear regression of the variable on the categorical integer coded VEGF-C variable, i.e. a test for linear trend across VEGF-C categories. A χ^2 test was applied for the non-ordinal St Gallen Classification. Logistic regression was used to evaluate associations with the binary outcome LNM. The joint predictive value of variables in multivariable logistic regression models was assessed using ROC-analysis, and discrimination was summarized as AUC (area under the ROC curve). Net Benefit was evaluated using decision curve analysis, and prognostic value was examined using Kaplan-Meier survival estimates, log-rank tests and Cox proportional hazards regression. All statistical tests presented are two-sided. P-values, which were not adjusted for multiple comparisons, should be interpreted as measures of evidence rather than compared to a fixed threshold for significance. Stata 19.0 (StataCorp LLC, TX, USA) was used for all the statistical calculations.

Declarations

Data Avaibility

The data that support the findings of this study are not openly available due to reasons of sensitivity and are available from the corresponding author upon reasonable request. Data are located in controlled access data storage a Lund University. All scripts used in this study have been deposited at https://github.com/rolnylab/Jeannot-Edvardsson-BreastCancer-Stromal-VEGFC-LymphNode/tree/main; DOI link found at https://doi.org/10.5281/zenodo.18803748

Author contribution:

LR: conceptualization, funding acquisition, methodology, supervision,

writing-original draft, writing-review, and editing; **CR:** conceptualization, funding acquisition, methodology, supervision, writing-original draft, writing-review, and editing; **OH:** investigation, formal analysis, writing-original draft, writing-review, and editing; **BÖ:** investigation, writing-review, and editing; **CB** investigation, writing-review, and editing. **AML:** investigation, writing-review, and editing. **EE:** conceptualization, formal analysis, writing-review, and editing; **POB:** conceptualization, formal analysis, methodology, supervision, visualization, writing-review, and editing; **LF:** methodology, investigation, writing-review, and editing; **PJ:** conceptualization, investigation, methodology, visualization, writing-review, and editing

Acknowledgments

To CR: gratefully acknowledge the support by Mrs. Berta Kamprad's Cancer Foundation to the L2CancerBridge program at CREATE Health Cancer Centre The Bertha Kamprad Foundation FBKS-2024-35 -(607), Crafoord foundation PR20241102. Swedish Research Council VR 2021-01149, Swedish Cancer Association: CAN 2022/2384 and 25/4742 . LR: The Erling Persson Foundation (22/1004), The Sjöberg Foundation (2023-01-03:14), The Governmental Funding for Clinical Research (22/40304), The Swedish Research Council (2020-01491; 2025-02438),

The Swedish Cancer Society (22-2137; 25-4514), The Skåne University Hospital Funds (24/25-792522), The Bertha Kamprad Foundation (FBKS-2022-20).

Conflict of Interest

The authors declare no conflict of interest.

Research Resource Identifiers

Reagents/Instruments/Software	Source	Identifier
anti-VEGF-C antibody (clone E6)	Santa Cruz Biotechnology	Cat# sc-374628; RRID:AB_11012156
OmniMap HRP-conjugated anti-mouse	Roche Diagnostics	Cat# 760-4310; RRID:AB_2885182
anti-panCK antibody (clone: AE1/3)	Agilent Technologies	Cat #M3515; RRID:AB_2132885
Ventana DISCOVERY ultra	Roche Diagnostics	Cat# 750-601; RRID:SCR_021254
Cell Conditioning 1 (CC1)	Roche Diagnostics	Cat# 950-500
ChromoMap DAB Kit (RUO), DISCOVERY	Roche Diagnostics	Cat# 760-159
Hematoxylin II	Roche Diagnostics	Cat# 790-2208
NanoZoomer S60 Digital Slide Scanner	Hamamatsu Photonics	RRID:SCR_022537
PhenoImager HT	Akoya	RRID:SCR_023772
QuPath	https://qupath.github.io	RRID:SCR_018257
R	https://www.r-project.org	RRID:SCR_001905
RStudio	https://posit.co/	RRID:SCR_000432
STATA	StataCorp LLC	RRID:SCR_012763

References

1. Appelgren, M. *et al.* Patient-reported outcomes one year after positive sentinel lymph node biopsy with or without axillary lymph node dissection in the randomized SENOMAC trial. *Breast* **63**, 16-23 (2022). https://doi.org:10.1016/j.breast.2022.02.013
2. Gentilini, O. D. *et al.* Sentinel Lymph Node Biopsy vs No Axillary Surgery in Patients With Small Breast Cancer and Negative Results on Ultrasonography of Axillary Lymph Nodes: The SOUND Randomized Clinical Trial. *JAMA Oncol* **9**, 1557-1564 (2023). https://doi.org:10.1001/jamaoncol.2023.3759
3. Reimer, T. *et al.* Axillary Surgery in Breast Cancer - Primary Results of the INSEMA Trial. *N Engl J Med* **392**, 1051-1064 (2025). https://doi.org:10.1056/NEJMoa2412063
4. Dihge, L., Ohlsson, M., Eden, P., Bendahl, P. O. & Ryden, L. Artificial neural network models to predict nodal status in clinically node-negative breast cancer. *BMC Cancer* **19**, 610 (2019). https://doi.org:10.1186/s12885-019-5827-6
5. Skarping, I. *et al.* Retrospective validation study of an artificial neural network-based preoperative decision-support tool for noninvasive lymph node staging (NILS) in women with primary breast cancer (ISRCTN14341750). *BMC Cancer* **24**, 86 (2024). https://doi.org:10.1186/s12885-024-11854-1
6. Banerjee, K. *et al.* VEGF-C-expressing TAMs rewire the metastatic fate of breast cancer cells. *Cell Rep* **42**, 113507 (2023). https://doi.org:10.1016/j.celrep.2023.113507
7. de Boniface, J. *et al.* Omitting Axillary Dissection in Breast Cancer with Sentinel-Node Metastases. *N Engl J Med* **390**, 1163-1175 (2024). https://doi.org:10.1056/NEJMoa2313487
8. Park, K. U. *et al.* Sentinel Lymph Node Biopsy in Early-Stage Breast Cancer: ASCO Guideline Update. *J Clin Oncol* **43**, 1720-1741 (2025). https://doi.org:10.1200/JCO-25-00099

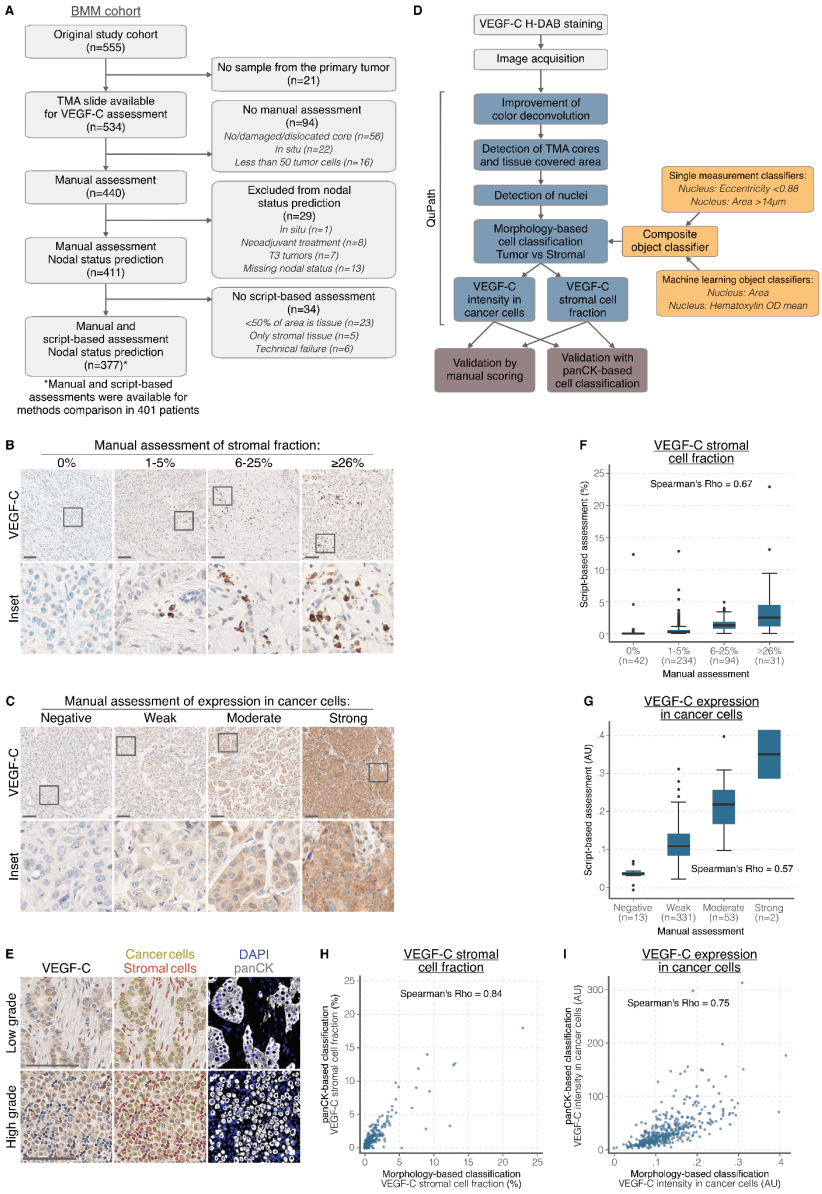
9. Parsons, A. *et al.* Cell populations in human breast cancers are molecularly and biologically distinct with age. *Nat Aging* **5**, 2546-2563 (2025). https://doi.org:10.1038/s43587-025-00984-1
10. Falck, A. K. *et al.* Analysis of and prognostic information from disseminated tumour cells in bone marrow in primary breast cancer: a prospective observational study. *BMC Cancer* **12**, 403 (2012). https://doi.org:10.1186/1471-2407-12-403
11. Falck, A. K. *et al.* Biomarker expression and St Gallen molecular subtype classification in primary tumours, synchronous lymph node metastases and asynchronous relapses in primary breast cancer patients with 10 years' follow-up. *Breast Cancer Res Treat* **140**, 93-104 (2013). https://doi.org:10.1007/s10549-013-2617-8
12. Lundgren, C. *et al.* Tumour-infiltrating lymphocytes as a prognostic and tamoxifen predictive marker in premenopausal breast cancer: data from a randomised trial with long-term follow-up. *Breast Cancer Res* **22**, 140 (2020). https://doi.org:10.1186/s13058-020-01364-w
13. Jorgensen, C. L. T. *et al.* PAM50 Intrinsic Subtype Profiles in Primary and Metastatic Breast Cancer Show a Significant Shift toward More Aggressive Subtypes with Prognostic Implications. *Cancers (Basel)* **13** (2021). https://doi.org:10.3390/cancers13071592
14. Larsson, A. M. *et al.* Longitudinal enumeration and cluster evaluation of circulating tumor cells improve prognostication for patients with newly diagnosed metastatic breast cancer in a prospective observational trial. *Breast Cancer Res* **20**, 48 (2018). https://doi.org:10.1186/s13058-018-0976-0
15. Bankhead, P. *et al.* QuPath: Open source software for digital pathology image analysis. *Sci Rep* **7**, 16878 (2017). https://doi.org:10.1038/s41598-017-17204-5

Tables

Tables 1 to 4 are available in the Supplementary Files section.

Figures

Fig. 1: Script-based morphometric approach enables automated quantification of the VEGF-C stromal fraction and cancer-cell VEGF-C expression

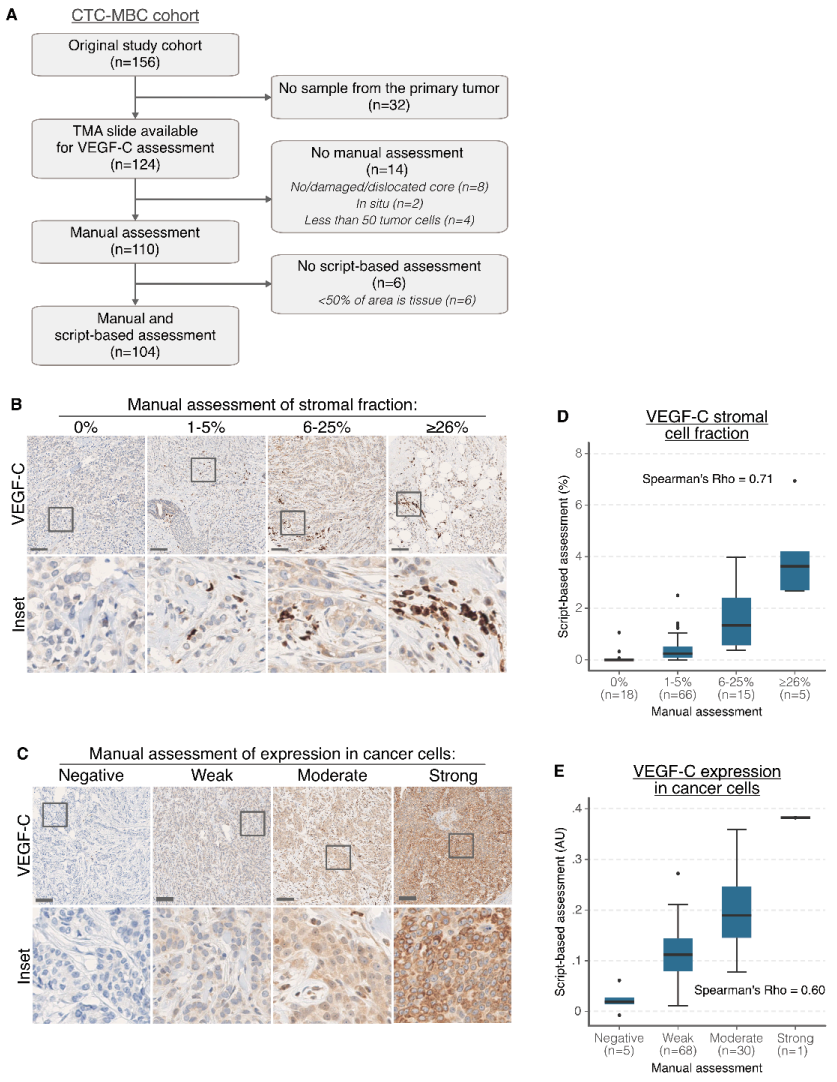


(A) Flow chart illustrating the selection of patients for the Bone Marrow Metastasis cohort (BMM).
(**B-C**) Representative immunohistochemistry images demonstrating manual scoring of the VEGF-C stromal fraction **(B)** and VEGF-C expression in cancer cells **(C)**. **(D)** Overview of the computational pipeline used to detect VEGF-C–positive stromal cells and quantify VEGF-C expression in cancer cells. **(E)** Representative regions showing VEGF-C staining (left), automated classification into cancer versus stromal cells (middle), and corresponding fluorescent staining for DAPI and pan-cytokeratin (panCK) (right).
(F-G) Boxplots comparing script-based morphometric quantification with manual assessment for the VEGF-C stromal fraction **(F)** and VEGF-C expression in cancer cells **(G)**. **(H)** Dot plot comparing the VEGF-C stromal fraction obtained using panCK-based cell classification on fluorescent staining with the script-based morphometric approach applied to H-DAB staining.

Figure 1

See image above for figure legend.

Fig. 2: Validation of the automated morphometric approach in the CTC-MBC cohort

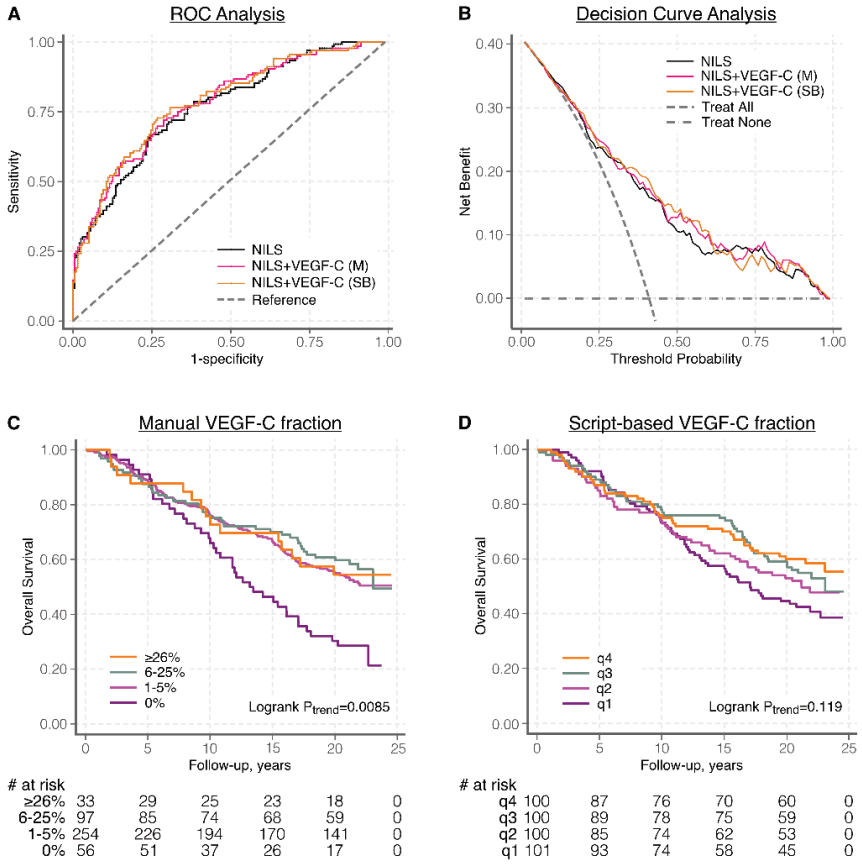


(A) Flow chart illustration the selection of patients for the Circulating Tumor cells in Metastatic Breast Cancer cohort (CTC-MBC).
(B-C) Representative immunohistochemistry images demonstrating manual scoring of the VEGF-C stromal fraction (B) and VEGF-C expression in cancer cells (C).
(D-E) Boxplots comparing script-based morphometric quantification with manual assessment for the VEGF-C stromal fraction (D) or VEGF-C expression in cancer cells (E). (F) Dot plot comparing the VEGF-C stromal fraction obtained using panCK-based cell classification on fluorescent staining with the script-based morphometric approach applied to H-DAB staining.

Figure 2

See image above for figure legend.

Fig. 3: Discrimination of nodal status in multivariable prediction models with and without stromal fraction of VEGF-C, net benefit of these models, and associations with prognosis.



(A) ROC-analysis comparing the discriminatory performance of three prediction models for nodal status: a reference model (NILS) and two models with stromal VEGF-C added, either manual (M) or script-based (SB) assessment. (B) Net benefit for the three models compared to the strategies of performing sentinel lymph node biopsy in all patients or in none. (C-D) Stromal VEGF-C fraction in relation to overall survival: (C) manually assessed (4 categories) and (D) script-based assessment (quartiles).

Figure 3

See image above for figure legend.

Supplementary Files

This is a list of supplementary files associated with this preprint. Click to download.

- JeannotTabels14.pdf